Array-Gain Constraint Minimum-Norm Spatial Filter With Recursively Updated Gram Matrix For Biomagnetic Source Imaging

Isamu Kumihashi and Kensuke Sekihara*, *Fellow, IEEE*

***Abstract*—This paper proposes a novel spatial filter for biomagnetic source imaging. The proposed spatial filter is derived based on a modified version of the minimum-norm spatial filter and is designed to have a performance close to that of the adaptive minimum-variance spatial filter through the use of an estimated covariance matrix. In this method, the theoretical form of the measurement covariance matrix is estimated as an updated gram matrix in a recursive procedure. Since the proposed method does not use the sample covariance matrix, it is free of the well-known weaknesses of the minimum-variance spatial filter, namely, the proposed spatial filter does not require a large number of time samples, and it can even be applied to single-time-sample data. It is also robust to source correlation. We have validated the method's effectiveness by our computer simulations as well as through experiments using auditory-evoked magnetoencephalographic data.**

***Index Terms*—Biomagnetic source reconstruction, magnetoencephalography (MEG), minimum-norm method, minimum-variance spatial filter, source reconstruction, spatial filter.**

I. Introduction

THE SPATIAL filter is a popular method used to reconstruct a source distribution from bioelectromagnetic data [1]. It is a linear operator that applies a set of linear weights to measured data to obtain a source reconstruction. When the weight of a spatial filter only depends on the geometry of the measurements, such a spatial filter is referred to as a nonadaptive spatial filter, which includes the minimum-norm-based filters discussed in Section II-B. In contrast to nonadaptive spatial filters, the weight of an adaptive spatial filter depends not only on the measurement geometry but also on the measurement covariance matrix. A representative adaptive spatial filter is the minimum-variance spatial filter described in Section II-C.

It is generally true that a nonadaptive spatial filter has a large source location bias, particularly when applied to 3-D volume reconstruction [1], [2]. In contrast, the source location bias of an adaptive spatial filter is generally small and can provide reasonable 3-D source reconstruction [1], [2]. The spatial resolution of an adaptive spatial filter is significantly higher than that of nonadaptive spatial filters [1], [2].

However, adaptive spatial filters have well-known weaknesses. First, since the computation of their weights requires a sample covariance matrix of the measured data, a large number of time samples are needed to obtain an accurate sample covariance matrix. In many cases of bioelectromagnetic measurements, however, it is rather difficult to obtain a large number of time samples. Second, the adaptive spatial filter is known to be sensitive to the source correlation, and it generally fails to reconstruct source activities when they are highly correlated [3], [4]. Typical cases include the bilateral activation of auditory cortices [5].

In this paper, we propose a novel spatial filter based on a modified version of the minimum-norm filter, called the array-gain constrained minimum-norm filter. The proposed method is designed to estimate the theoretical form of the measurement covariance matrix through recursively updating the gram matrix. Thus, the proposed method is termed "array-gain constraint minimum-norm filter with recursively updated gram matrix" abbreviated as the AGMN-RUG spatial filter in this paper. The proposed AGMN-RUG method is able to provide 3-D volume reconstruction with a spatial resolution considerably higher than that of existing minimum-norm-based methods. Nonetheless, the method is free of the aforementioned weaknesses occurring with adaptive spatial filters, because it does not depend on the sample covariance matrix. The method is also robust to the source correlation, and this robustness can be seen in our computer simulation as well as in our experiments using auditory-evoked magnetoencephalographic (MEG) data.

After presenting reviews of the nonadaptive minimum-norm filters and the adaptive minimum-variance filters in Section II, this paper proposes a novel AGMN-RUG spatial filter in Section III. The proposed spatial filter is validated by our computer simulation in Section IV and by applications to auditory-evoked MEG data presented in Section V. Throughout this paper, plain italics indicate scalars, lower case boldface italics indicate vectors, and upper case boldface italics indicate matrices.

II. Formulation of Representative Spatial Filters

A. Spatial Filter Source Reconstruction

Let us define the biomagnetic field measured by the mth sensor at time t as $b_m(t)$, and the measured data as the column vector $\boldsymbol{b}(t) = [b_1(t), b_2(t), \ldots, b_M(t)]^T$. Here, M is the total number

Manuscript received July 31, 2009; revised November 15, 2009; accepted December 16, 2009. Date of publication February 17, 2010; date of current version May 14, 2010. This work was supported by Grants-in-Aid from the Ministry of Education, Science, Culture and Sports in Japan (C20500394). *Asterisk indicates corresponding author*.

I. Kumihashi is with the Department of Systems Design and Engineering, Tokyo Metropolitan University, Tokyo 191-0065, Japan (e-mail: kumihashi136_ac@yahoo.co.jp).

*K. Sekihara is with the Department of Systems Design and Engineering, Tokyo Metropolitan University, Tokyo 191-0065, Japan (e-mail: ksekiha@cc.tmit.ac.jp).

Color versions of one or more of the figures in this paper are available online at http://ieeexplore.ieee.org.

Digital Object Identifier 10.1109/TBME.2010.2040735

of sensors and the superscript T indicates the matrix transpose. A spatial location is represented by a 3-D vector $\boldsymbol{r}$, as $\boldsymbol{r} = (x, y, z)$. A source vector at $\boldsymbol{r}$ and time t is defined as a 3-D column vector $\boldsymbol{s}(\boldsymbol{r}, t)$, where $\boldsymbol{s}(\boldsymbol{r}, t) = [s_x(\boldsymbol{r}, t), s_y(\boldsymbol{r}, t), s_z(\boldsymbol{r}, t)]^T$, and $s_x(\boldsymbol{r}, t)$, $s_y(\boldsymbol{r}, t)$, and $s_z(\boldsymbol{r}, t)$ are the x, y, and z components of the source vector $\boldsymbol{s}(\boldsymbol{r}, t)$.

We denote the outputs of the mth sensor as $l_m^x(\boldsymbol{r})$, $l_m^y(\boldsymbol{r})$, and $l_m^z(\boldsymbol{r})$ when the unit-magnitude source at $\boldsymbol{r}$ is directed in the x, y, and z directions, respectively. Then, the column vectors $\boldsymbol{l}_x(\boldsymbol{r})$, $\boldsymbol{l}_y(\boldsymbol{r})$, and $\boldsymbol{l}_z(\boldsymbol{r})$ are defined as

$$\boldsymbol{l}_i(\boldsymbol{r}) = [l_1^i(\boldsymbol{r}), l_2^i(\boldsymbol{r}), \ldots, l_M^i(\boldsymbol{r})]^T \tag{1}$$

where $i = x, y$ or z. The vectors, $\boldsymbol{l}_x(\boldsymbol{r})$, $\boldsymbol{l}_y(\boldsymbol{r})$, and $\boldsymbol{l}_z(\boldsymbol{r})$, express the sensor array sensitivity for a source at $\boldsymbol{r}$ directed in the x, y, and z directions. The lead-field matrix is expressed as the $M \times 3$ matrix:

$$\boldsymbol{L}(\boldsymbol{r}) = [\boldsymbol{l}_x(\boldsymbol{r}), \boldsymbol{l}_y(\boldsymbol{r}), \boldsymbol{l}_z(\boldsymbol{r})]. \tag{2}$$

This matrix $\boldsymbol{L}(\boldsymbol{r})$ represents the sensitivity of the whole sensor array for a source at $\boldsymbol{r}$. The relationship between the measurement vector $\boldsymbol{b}(t)$ and the 3-D source vector $\boldsymbol{s}(\boldsymbol{r}, t)$ is then expressed as

$$\boldsymbol{b}(t) = \int_\Omega \boldsymbol{L}(\boldsymbol{r}) \boldsymbol{s}(\boldsymbol{r}, t)\, d^3 r \tag{3}$$

where $d^3 r$ indicates the volume element, and the integral is performed over the entire space within which sources may exist. This space is referred to as the source space and denoted Ω in this paper.

Using the measurement vector $\boldsymbol{b}(t)$, the spatial filter reconstructs the source vector $\boldsymbol{s}(\boldsymbol{r}, t)$ using

$$\widehat{\boldsymbol{s}}(\boldsymbol{r}, t) = [\widehat{s}_x(\boldsymbol{r}, t), \widehat{s}_y(\boldsymbol{r}, t), \widehat{s}_z(\boldsymbol{r}, t)]^T = \boldsymbol{W}^T(\boldsymbol{r}) \boldsymbol{b}(t). \tag{4}$$

where $\widehat{\boldsymbol{s}}(\boldsymbol{r}, t)$ is the estimated source vector at $\boldsymbol{r}$ and time t. In (4), the weight matrix $\boldsymbol{W}(\boldsymbol{r})$ is an $M \times 3$ matrix defined as

$$\boldsymbol{W}(\boldsymbol{r}) = [\boldsymbol{w}_x(\boldsymbol{r}), \boldsymbol{w}_y(\boldsymbol{r}), \boldsymbol{w}_z(\boldsymbol{r})] \tag{5}$$

where $M \times 1$ weight vectors $\boldsymbol{w}_x(\boldsymbol{r})$, $\boldsymbol{w}_y(\boldsymbol{r})$, and $\boldsymbol{w}_z(\boldsymbol{r})$, respectively detect $\widehat{s}_x(\boldsymbol{r}, t)$, $\widehat{s}_y(\boldsymbol{r}, t)$, and $\widehat{s}_z(\boldsymbol{r}, t)$. This weight matrix characterizes the properties of the spatial filter. Combining (3) and (4), we derive (omitting explicit time notation t)

$$\widehat{\boldsymbol{s}}(\boldsymbol{r}) = \int_\Omega \boldsymbol{W}^T(\boldsymbol{r}) \boldsymbol{L}(\boldsymbol{r}') \boldsymbol{s}(\boldsymbol{r}')\, d^3 r'. \tag{6}$$

Here, $\boldsymbol{W}^T(\boldsymbol{r}) \boldsymbol{L}(\boldsymbol{r}')$ is called the resolution kernel, and expresses the relationship between the true source distribution $\boldsymbol{s}(\boldsymbol{r})$ and the estimated source distribution $\widehat{\boldsymbol{s}}(\boldsymbol{r})$. One way of interpreting the resolution kernel is to consider it as a function of $\boldsymbol{r}'$ using a fixed $\boldsymbol{r}$. In such a case, $\boldsymbol{W}^T(\boldsymbol{r}) \boldsymbol{L}(\boldsymbol{r}')$, called the beam response, expresses the sensitivity of the spatial filter pointing at $\boldsymbol{r}$ to a source located at $\boldsymbol{r}'$. In other words (when $\boldsymbol{r} \neq \boldsymbol{r}'$), the beam response represents the gain on unwanted leakage signals from sources located elsewhere from the filter pointing location.

B. Minimum-Norm-Based Spatial Filters

Next, we show that the minimum-norm-based spatial filters can be derived using optimization formulations that force their beam responses to have an ideal delta-function-like shape [1], i.e, the weight matrix of the minimum-norm spatial filter is derived using

$$\boldsymbol{W}(\boldsymbol{r}) = \arg\min_{\boldsymbol{W}(\boldsymbol{r})} \quad \mathcal{F}(\boldsymbol{W}) \tag{7}$$

where

$$\mathcal{F}(\boldsymbol{W}) = \int_\Omega \mathrm{tr}\{ \left[\boldsymbol{W}^T(\boldsymbol{r}) \boldsymbol{L}(\boldsymbol{r}') - \delta(\boldsymbol{r} - \boldsymbol{r}') \boldsymbol{I}\right] \left[\boldsymbol{W}^T(\boldsymbol{r}) \boldsymbol{L}(\boldsymbol{r}') - \delta(\boldsymbol{r} - \boldsymbol{r}') \boldsymbol{I}\right]^T \} \, d^3 r'. \tag{8}$$

Here, $\boldsymbol{I}$ is the identity matrix, $\mathrm{tr}\{\cdot\}$ indicates the matrix trace, and $\delta(\boldsymbol{r})$ is the delta function. The cost function $\mathcal{F}(\boldsymbol{W})$ in (8) indicates the total power of the leakage signals. Therefore, using the previous optimization, we wish to derive a spatial filter that passes the signal from the pointing location $\boldsymbol{r}$ but minimizes the total power of the leakages from all other locations.

To find the $\boldsymbol{W}(\boldsymbol{r})$ that minimizes this $\mathcal{F}(\boldsymbol{W})$, we calculate the derivative $\partial \mathcal{F}(\boldsymbol{W}) / \partial \boldsymbol{W}(\boldsymbol{r})$ and set it to zero, i.e.,

$$\begin{aligned} \frac{\partial \mathcal{F}(\boldsymbol{W})}{\partial \boldsymbol{W}(\boldsymbol{r})} &= 2 \int_\Omega \left[\boldsymbol{L}(\boldsymbol{r}') \boldsymbol{L}^T(\boldsymbol{r}') \boldsymbol{W}(\boldsymbol{r}) - \boldsymbol{L}(\boldsymbol{r}') \delta(\boldsymbol{r} - \boldsymbol{r}')\right] d^3 r' \\ &= 2 \left[\int_\Omega \boldsymbol{L}(\boldsymbol{r}') \boldsymbol{L}^T(\boldsymbol{r}')\, d^3 r'\right] \boldsymbol{W}(\boldsymbol{r}) - 2 \boldsymbol{L}(\boldsymbol{r}) \\ &= 2 \left[\boldsymbol{G} \boldsymbol{W}(\boldsymbol{r}) - \boldsymbol{L}(\boldsymbol{r})\right] = 0 \end{aligned} \tag{9}$$

where $\boldsymbol{G}$, called the gram matrix, is an $M \times M$ matrix defined as

$$\boldsymbol{G} = \int_\Omega \boldsymbol{L}(\boldsymbol{r}) \boldsymbol{L}^T(\boldsymbol{r})\, d^3 r. \tag{10}$$

From (9), we can derive the weight matrix given by

$$\boldsymbol{W}(\boldsymbol{r}) = \boldsymbol{G}^{-1} \boldsymbol{L}(\boldsymbol{r}). \tag{11}$$

The spatial filter in (11) is equal to the well-known minimum-norm spatial filter [6].

Several variants of the minimum-norm filter can be derived by adding some constraints to the optimization formulation in (7). An example of such constraint is one on the filter gain at the pointing location. We first consider the unit-gain constraint expressed as $\boldsymbol{W}^T(\boldsymbol{r}) \boldsymbol{L}(\boldsymbol{r}) = \boldsymbol{I}$. The constrained optimization is explicitly formulated, in this case, as

$$\boldsymbol{W}(\boldsymbol{r}) = \arg\min_{\boldsymbol{W}(\boldsymbol{r})} \mathcal{F}(\boldsymbol{W}), \quad \text{subject to} \quad \boldsymbol{W}^T(\boldsymbol{r}) \boldsymbol{L}(\boldsymbol{r}) = \boldsymbol{I} \tag{12}$$

where $\mathcal{F}(\boldsymbol{W})$ is defined in (8). The weight matrix satisfying (12) is known to have the following form:

$$\boldsymbol{W}(\boldsymbol{r}) = \boldsymbol{G}^{-1} \boldsymbol{L}(\boldsymbol{r}) [\boldsymbol{L}^T(\boldsymbol{r}) \boldsymbol{G}^{-1} \boldsymbol{L}(\boldsymbol{r})]^{-1}. \tag{13}$$

This spatial filter is called the unit-gain constraint minimum-norm filter reported in [7].

The constrained optimization,

$$\boldsymbol{W}(\boldsymbol{r}) = \arg\min_{\boldsymbol{W}(\boldsymbol{r})} \mathcal{F}(\boldsymbol{W}), \text{ subject to } \int_\Omega \left[\boldsymbol{W}^T(\boldsymbol{r}) \boldsymbol{L}(\boldsymbol{r}')\right] \left[\boldsymbol{W}^T(\boldsymbol{r}) \boldsymbol{L}(\boldsymbol{r}')\right]^T \, d^3 r' = \boldsymbol{I} \tag{14}$$

leads to the weight matrix expressed as

$$\boldsymbol{W}(\boldsymbol{r}) = \boldsymbol{G}^{-1}\boldsymbol{L}(\boldsymbol{r})[\boldsymbol{L}^T(\boldsymbol{r})\boldsymbol{G}^{-1}\boldsymbol{L}(\boldsymbol{r})]^{-1/2}. \quad (15)$$

This spatial filter is known as standardized low-resolution electromagnetic tomography (sLORETA) [8].

C. Minimum-Variance Spatial Filter

The minimum-variance spatial filter is a representative adaptive spatial filter, whose weight matrix is formulated using the measurement covariance matrix $\boldsymbol{R}$. Using the unit-gain constraint, $\boldsymbol{W}^T(\boldsymbol{r})\boldsymbol{L}(\boldsymbol{r}) = \boldsymbol{I}$, the weight matrix is derived using the optimization,

$$\boldsymbol{W}(\boldsymbol{r}) = \arg\min_{\boldsymbol{W}(\boldsymbol{r})} \mathrm{tr}\{\boldsymbol{W}^T\boldsymbol{R}\boldsymbol{W}\}, \quad \text{subject to} \quad \boldsymbol{W}^T(\boldsymbol{r})\boldsymbol{L}(\boldsymbol{r}) = \boldsymbol{I}. \quad (16)$$

The resultant weight matrix is expressed as [3],

$$\boldsymbol{W}(\boldsymbol{r}) = \boldsymbol{R}^{-1}\boldsymbol{L}(\boldsymbol{r})[\boldsymbol{L}^T(\boldsymbol{r})\boldsymbol{R}^{-1}\boldsymbol{L}(\boldsymbol{r})]^{-1}. \quad (17)$$

This minimum-variance spatial filter is known to have significantly higher spatial resolution and much smaller source location bias, compared to the minimum-norm-based spatial filters mentioned in the preceding subsection [2].

For biomagnetic imaging, the norm of the lead field $\|\boldsymbol{L}(\boldsymbol{r})\|$ is spatially nonuniform and the minimum-variance spatial filter is affected by this nonuniformity of the lead-field norm, as can be seen in the weight expression in (17). Particularly when the spherical homogeneous conductor model [9] is used for computing the lead field, the source reconstruction results contain a false intensity increase around the center of the sphere [1], because $\|\boldsymbol{L}(\boldsymbol{r})\|$ becomes zero and the weight becomes infinity at the center.

When $\|\boldsymbol{L}(\boldsymbol{r})\|$ is spatially nonuniform, instead of using the unit-gain constraint $\boldsymbol{W}^T(\boldsymbol{r})\boldsymbol{L}(\boldsymbol{r}) = \boldsymbol{I}$, it is more reasonable to use the constraint $\boldsymbol{W}^T(\boldsymbol{r})\boldsymbol{L}(\boldsymbol{r}) = \boldsymbol{\Lambda}$, where

$$\boldsymbol{\Lambda} = \begin{bmatrix} \|\boldsymbol{l}_x(\boldsymbol{r})\| & 0 & 0 \\ 0 & \|\boldsymbol{l}_y(\boldsymbol{r})\| & 0 \\ 0 & & \|\boldsymbol{l}_z(\boldsymbol{r})\| \end{bmatrix}. \quad (18)$$

In this case, the weight matrix is expressed as

$$\boldsymbol{W}(\boldsymbol{r}) = \boldsymbol{R}^{-1}\widetilde{\boldsymbol{L}}(\boldsymbol{r})[\widetilde{\boldsymbol{L}}^T(\boldsymbol{r})\boldsymbol{R}^{-1}\widetilde{\boldsymbol{L}}(\boldsymbol{r})]^{-1} \quad (19)$$

where $\widetilde{\boldsymbol{L}}(\boldsymbol{r})$ is the lead-field matrix consisting of the normalized columns, i.e.,

$$\widetilde{\boldsymbol{L}}(\boldsymbol{r}) = \left[\frac{\boldsymbol{l}_x(\boldsymbol{r})}{\|\boldsymbol{l}_x(\boldsymbol{r})\|}, \frac{\boldsymbol{l}_y(\boldsymbol{r})}{\|\boldsymbol{l}_y(\boldsymbol{r})\|}, \frac{\boldsymbol{l}_z(\boldsymbol{r})}{\|\boldsymbol{l}_z(\boldsymbol{r})\|}\right]. \quad (20)$$

In (19), the weight is independent of the norm of the lead field, and we can avoid the artifacts due to the nonuniformity of the lead-field norm. Since $\|\boldsymbol{l}_x(\boldsymbol{r})\|$, $\|\boldsymbol{l}_y(\boldsymbol{r})\|$, and $\|\boldsymbol{l}_z(\boldsymbol{r})\|$ represent the gains of the sensor array for a source directed in the x-, y-, and z-directions, the constraint $\boldsymbol{W}^T(\boldsymbol{r})\boldsymbol{L}(\boldsymbol{r}) = \boldsymbol{\Lambda}$ is called the array-gain constraint, and the spatial filter in (19) is called the array-gain (constraint) minimum-variance filter.

The weight matrices of the minimum-variance filters in (17) and (19) contain the covariance matrix $\boldsymbol{R}$. When computing these weights, a sample covariance estimate $\widehat{\boldsymbol{R}}$ is used for $\boldsymbol{R}$, and a large number of time samples are generally needed to obtain an accurate sample covariance matrix. However, in many bioelectromagnetic applications, it is difficult to obtain a large number of time samples. In the following section, we develop a spatial filter that outperforms the minimum-norm-based filters without using the sample covariance matrix. We derive an expression for $\boldsymbol{R}$ needed in our arguments in the next section. Using (3), the measurement covariance matrix is expressed as

$$\boldsymbol{R} = \langle \boldsymbol{b}(t)\boldsymbol{b}^T(t)\rangle = \int_\Omega \boldsymbol{L}(\boldsymbol{r})\langle \boldsymbol{s}(\boldsymbol{r},t)\boldsymbol{s}^T(\boldsymbol{r},t)\rangle \boldsymbol{L}^T(\boldsymbol{r})d\boldsymbol{r} \quad (21)$$

where $\langle\cdot\rangle$ indicates averaging. This expression for $\boldsymbol{R}$ is used in deriving the spatial filter proposed in the next section.

III. Proposed AGMN-RUG Spatial Filter

The proposed spatial filter is based on the array-gain-constraint minimum-norm filter, which is derived using the following optimization:

$$\boldsymbol{W}(\boldsymbol{r}) = \arg\min_{\boldsymbol{W}(\boldsymbol{r})} \mathcal{F}(\boldsymbol{W}), \quad \text{subject to} \quad \boldsymbol{W}^T(\boldsymbol{r})\boldsymbol{L}(\boldsymbol{r}) = \boldsymbol{\Lambda} \quad (22)$$

where $\boldsymbol{\Lambda}$ is the gain matrix defined in (18), and the cost function $\mathcal{F}(\boldsymbol{W})$ is defined, in this case, as

$$\mathcal{F}(\boldsymbol{W}) = \int_\Omega \mathrm{tr}\{\left[\boldsymbol{W}^T(\boldsymbol{r})\boldsymbol{L}(\boldsymbol{r}') - \delta(\boldsymbol{r}-\boldsymbol{r}')\boldsymbol{\Lambda}\right]\boldsymbol{P}(\boldsymbol{r}') \left[\boldsymbol{W}^T(\boldsymbol{r})\boldsymbol{L}(\boldsymbol{r}') - \delta(\boldsymbol{r}-\boldsymbol{r}')\boldsymbol{\Lambda}\right]^T\} d^3r' \quad (23)$$

where $\boldsymbol{P}(\boldsymbol{r}')$ is a 3×3 positive semidefinite matrix. This $\boldsymbol{P}(\boldsymbol{r}')$ is a matrix weighting function that controls location-dependent weighting when the resolution kernel is optimized. The resultant spatial filter is derived as

$$\boldsymbol{W}(\boldsymbol{r}) = \bar{\boldsymbol{G}}^{-1}\widetilde{\boldsymbol{L}}(\boldsymbol{r})[\widetilde{\boldsymbol{L}}^T(\boldsymbol{r})\bar{\boldsymbol{G}}^{-1}\widetilde{\boldsymbol{L}}(\boldsymbol{r})]^{-1} \quad (24)$$

where

$$\bar{\boldsymbol{G}} = \int_\Omega \boldsymbol{L}(\boldsymbol{r})\boldsymbol{P}(\boldsymbol{r})\boldsymbol{L}^T(\boldsymbol{r})\, d^3r. \quad (25)$$

If we compare (24) with (19), it is the weight equation for the array-gain constraint minimum-variance filter. The only difference between (24) and (19) is the use of $\bar{\boldsymbol{G}}$, instead of $\boldsymbol{R}$. We may then compare $\bar{\boldsymbol{G}}$ [see (25)] and $\boldsymbol{R}$ [see (21)] and find that these two matrices are very similar and differ only in the manner of weighting in the integral, i.e., the covariance matrix $\boldsymbol{R}$ is expressed as the integral of $\boldsymbol{L}(\boldsymbol{r})\boldsymbol{L}^T(\boldsymbol{r})$, with the weighting of the source power matrix $\langle \boldsymbol{s}(\boldsymbol{r},t)\boldsymbol{s}^T(\boldsymbol{r},t)\rangle$. On the other hand, the gram matrix $\bar{\boldsymbol{G}}$ is given by the integral of $\boldsymbol{L}(\boldsymbol{r})\boldsymbol{L}^T(\boldsymbol{r})$, with the weighting of an arbitrary matrix function $\boldsymbol{P}(\boldsymbol{r})$.

Therefore, if we could use a $\boldsymbol{P}(\boldsymbol{r})$ that is similar to the source power matrix $\langle \boldsymbol{s}(\boldsymbol{r},t)\boldsymbol{s}^T(\boldsymbol{r},t)\rangle$, the gram matrix $\bar{\boldsymbol{G}}$ could approximate the covariance matrix $\boldsymbol{R}$, and consequently, the performance of the array-gain minimum-norm filter would approach the performance of the minimum-variance filter. However, since the true source distribution $\boldsymbol{s}(\boldsymbol{r})$ is unknown,

we propose using the estimated source distribution $\widehat{\boldsymbol{s}}(\boldsymbol{r})$ for computing $\boldsymbol{P}(\boldsymbol{r})$.

The proposed recursive algorithm is described in the following manner.

1) By setting an initial $\boldsymbol{P}(\boldsymbol{r})$ to be the identity matrix $\boldsymbol{I}$, the weight $\boldsymbol{W}(\boldsymbol{r})$ is derived using (24) and (25).
2) The estimated source distribution $\widehat{\boldsymbol{s}}(\boldsymbol{r}, t)$ is obtained using (4).
3) This $\widehat{\boldsymbol{s}}(\boldsymbol{r}, t)$ is then used to compute $\bar{\boldsymbol{G}}$ at each time point such that

$$\bar{\boldsymbol{G}} = \int_{\Omega} \boldsymbol{L}(\boldsymbol{r}) \left[\widehat{\boldsymbol{s}}(\boldsymbol{r}, t)\widehat{\boldsymbol{s}}^{T}(\boldsymbol{r}, t)\right] \boldsymbol{L}^{T}(\boldsymbol{r})\, d^3 r \qquad (26)$$

whereupon the weight matrix is updated using (24).
4) Finally, the updated source distribution is obtained using the updated weight matrix with (4).

This procedure is repeated until a stopping criterion is satisfied.

One important problem in practical applications is the influence of measurement noise. In biomagnetic measurements, the condition number of the gram matrix obtained in (26) is generally significantly large and the spatial filter in (24) is not robust to the measurement noise. Since the norm of the filter weight $\|\boldsymbol{W}(\boldsymbol{r})\|$ is the noise power gain of the spatial filter [1], one way to derive a spatial filter that is relatively tolerant to the measurement noise is to add an additional constraint that makes $\|\boldsymbol{W}(\boldsymbol{r})\|$ not greater than a certain bound, i.e., we derive such a spatial filter using

$$\boldsymbol{W}(\boldsymbol{r}) = \underset{\boldsymbol{W}(\boldsymbol{r})}{\arg\min}\, \mathcal{F}(\boldsymbol{W}), \text{ subject to } \quad \boldsymbol{W}^{T}(\boldsymbol{r})\boldsymbol{L}(\boldsymbol{r}) = \boldsymbol{\Lambda}, \quad \text{and} \quad \|\boldsymbol{W}(\boldsymbol{r})\| \leq W_B \qquad (27)$$

where the noise gain of the resultant spatial filter is not greater than the bound W_B [1]. This formulation leads to the weight expressed as

$$\boldsymbol{W}(\boldsymbol{r}) = \widehat{\boldsymbol{G}}^{-1}\widetilde{\boldsymbol{L}}(\boldsymbol{r})[\widetilde{\boldsymbol{L}}^{T}(\boldsymbol{r})\widehat{\boldsymbol{G}}^{-1}\widetilde{\boldsymbol{L}}(\boldsymbol{r})]^{-1} \qquad (28)$$

where

$$\widehat{\boldsymbol{G}} = \int_{\Omega} \boldsymbol{L}(\boldsymbol{r})\boldsymbol{P}(\boldsymbol{r})\boldsymbol{L}^{T}(\boldsymbol{r})\, d^3 r + \gamma \boldsymbol{I} = \bar{\boldsymbol{G}} + \gamma \boldsymbol{I}. \qquad (29)$$

The scalar parameter γ works as the regularization parameter determined based on the SNR in the measurements. We use this regularized version of the proposed spatial filter in the experiments in the following sections. In these experiments, we determine γ to be equal to the noise floor of the eigenvalue spectrum of the measurement covariance matrix, $\widehat{\boldsymbol{R}}$, i.e., we use γ that is equal to the mean of the noise-level eigenvalues of $\widehat{\boldsymbol{R}}$. Actually, considering the difference of the scaling between $\widehat{\boldsymbol{R}}$ and $\bar{\boldsymbol{G}}$, we derive γ such that

$$\gamma = \left[\frac{1}{K_n}\sum_{\text{noise}} \lambda_i\right] \frac{\|\bar{\boldsymbol{G}}\|}{\|\widehat{\boldsymbol{R}}\|} \qquad (30)$$

where $\sum_{\text{noise}} \lambda_i$ indicates the summation over the noise eigenvalues, and K_n is total number of those eigenvalues.

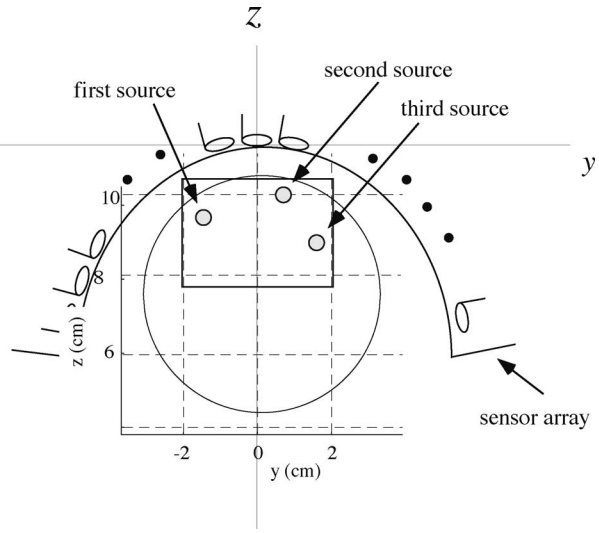

Fig. 1. Coordinate system and source-sensor configuration used in the computer simulation. The coordinate origin was set at the center of the sensor coil located at the center of the array. The plane at $x = 0$ cm is shown. The large circle shows the cross-section of the sphere used for the forward calculation, and the small circles show the locations of the three sources. The square shows the region for displaying the reconstruction results in Figs. 2– 7.

IV. Computer Simulation

A. Reconstruction From Single-Time-Sample Data

A computer simulation was conducted to check the performance of the proposed AGMN-RUG spatial filter. In this computer simulation, we used a sensor alignment of the Magnes 2500 (4-D Neuroimaging, Inc., San Diego, CA) whole-head sensor array, in which 148 sensors were arranged on a helmet-shaped surface. Three sources were assumed to exist on the vertical single plane: ($x = 0$ cm); their (y, z) coordinates chosen as $(-3.5, -6.5)$ cm, $(1.0, -5.0)$ cm, and $(4.0, -8.75)$ cm, respectively. The source-sensor configuration and the coordinate system are depicted in Fig. 1. The spherical homogeneous conductor model [9], with the sphere origin set at $(0, 0, -12)$ cm, was used for the forward calculation. First, the sensor data at a single time sample was calculated. Here, the intensities of the three sources were set equal in the sensor domain. Gaussian noise was added, and the SNR of the data was set to 16 where the SNR was defined as the ratio of the norm of the signal vector to the norm of the noise vector.

The source reconstruction was performed using sLORETA, and the proposed AGMN-RUG spatial filter. Here, sLORETA was chosen for comparison, because it is a method representative of existing nonadaptive methods and is able to perform 3-D volume reconstruction. The source space Ω was defined as the 3-D region between $-4 \leq x \leq 4$ cm, $-5 \leq y \leq 5$ cm, and $-11 \leq z \leq -3$ cm. The 3-D reconstruction was performed on Ω with a 1-cm voxel interval. The squared source intensity $|\widehat{\boldsymbol{s}}(\boldsymbol{r})|^2$ was plotted on the plane $x = 0$ cm on which the three sources were presumed to exist. The results from sLORETA and the proposed spatial filter are shown in Fig. 2(a) and (b). It can be clearly seen that the proposed spatial filter reconstructs the three sources at approximately correct locations. On

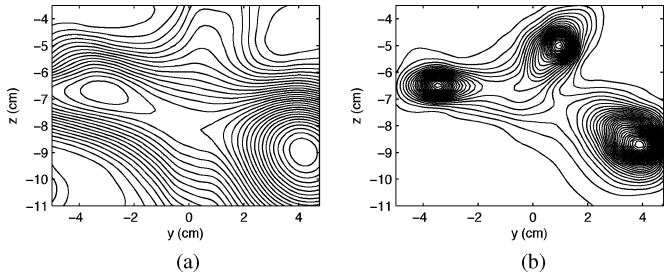

Fig. 2. Results of source reconstruction for single-time-sample data. (a) Results when the sLORETA spatial filter was applied. (b) Results when the proposed AGMN-RUG spatial filter was applied. The contours show the relative values of the squared source intensity $|\widehat{\boldsymbol{s}}(\boldsymbol{r})|^2$ on the plane $x = 0$ cm on which three sources exist.

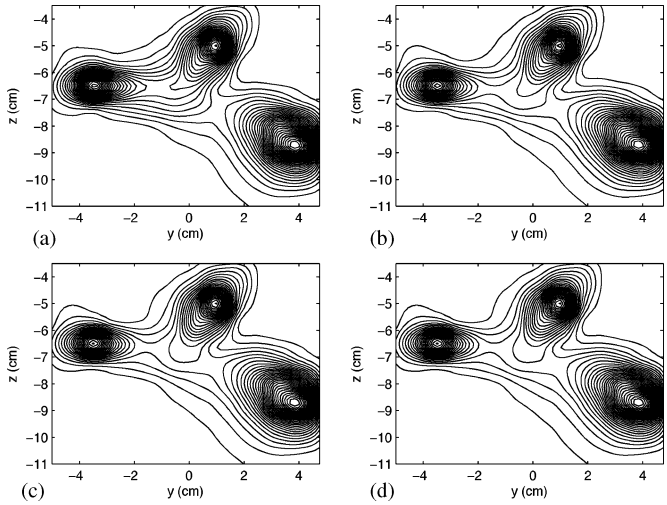

Fig. 3. Results of the source reconstruction obtained using the proposed AGMN-RUG spatial filter with four different iteration numbers. (a) Number of iterations was set to 4. (b) Number of iterations set to 16. (c) Number of iterations set to 256. (d) Number of iterations set to 1024. The contours show the relative values of the squared source intensity $|\widehat{\boldsymbol{s}}(\boldsymbol{r})|^2$ on the plane $x = 0$ cm.

the contrary, sLORETA produces blurred results, and fails to reconstruct the first and the second sources.

In this implementation of the proposed AGMN-RUG spatial filter, we set the number of iterations to eight. Since this number was empirically determined, we checked how the proposed method is sensitive to the number of iterations by using the same single-time-sample data with four different iteration numbers. The results obtained with iteration numbers of 4, 16, 256, and 1024 are shown in Fig. 3(a), (b), (c), and (d), respectively. It can be seen that these four sets of results are nearly identical, suggesting that the method is rather stable with regard to the number of iterations. We present a brief discussion regarding this stability of the proposed method in Section VI.

B. Reconstruction From Spatiotemporal Dataset

Next, we performed experiments on the reconstruction based on a spatiotemporal dataset. The three time courses shown in Fig. 4 were assigned to the three sources, and the spatiotemporal data were generated over 200 time samples. These three time courses are denoted $s_1(t)$, $s_2(t)$, and $s_3(t)$. These time courses

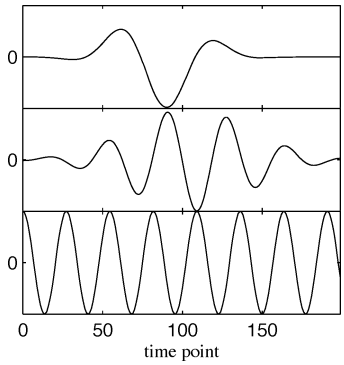

Fig. 4. (Top to bottom) Time courses $s_1(t)$, $s_2(t)$, and $s_3(t)$, used for generating the spatiotemporal dataset. The dataset was generated over 200 time samples. The abscissa indicates the time samples and the ordinate indicates the relative amplitudes.

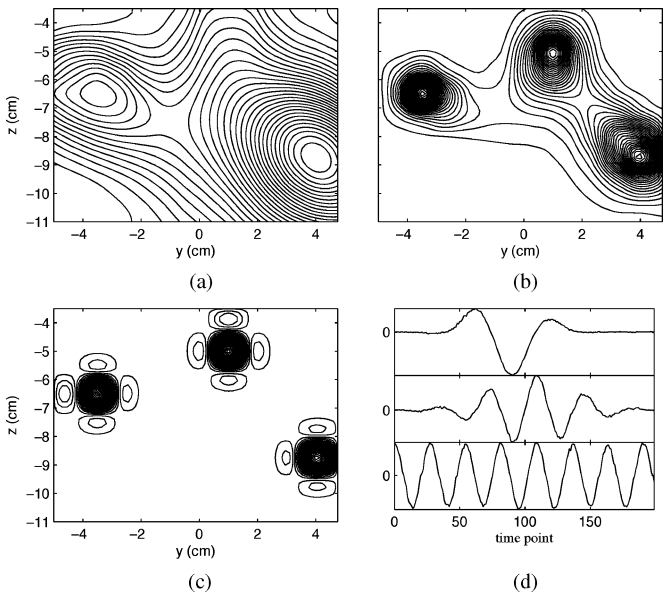

Fig. 5. Results of source reconstruction for the spatiotemporal data. (a) Results when the sLORETA spatial filter was applied. (b) Results when the proposed AGMN-RUG spatial filter was applied. (c) Results when the minimum-variance spatial filter was applied. The contours show the relative values of the squared source intensity $\langle|\widehat{\boldsymbol{s}}(\boldsymbol{r},t)|^2\rangle$ on the plane $x = 0$ cm, where $\langle\cdot\rangle$ indicates the average over the 200 time samples. (d) Reconstructed time courses of the three sources obtained using the proposed AGMN-RUG spatial filter. The three time courses are the time courses at voxels that give the three maxima in (b).

are largely uncorrelated and the correlation coefficients between any pair of the three are less than 0.1. The SNR was set equal to 16 (where the SNR was defined as the ratio of the Frobenius norm of the signal matrix to that of the noise matrix).

We applied sLORETA, the proposed spatial filter, and the minimum-variance spatial filter, to this spatiotemporal dataset. The source-power distribution $\langle|\widehat{\boldsymbol{s}}(\boldsymbol{r},t)|^2\rangle$ (where the notation $\langle\cdot\rangle$ indicates the average over the 200 time samples), was reconstructed over the source space Ω with a voxel interval of 1 cm, and the results for the plane $x = 0$ cm are displayed in panels (a), (b), and (c) of Fig. 5. When implementing the proposed spatial filter, the number of iterations was set to eight. The sample covariance matrix was computed using all 200 time samples when implementing the minimum-variance filter reconstruction.

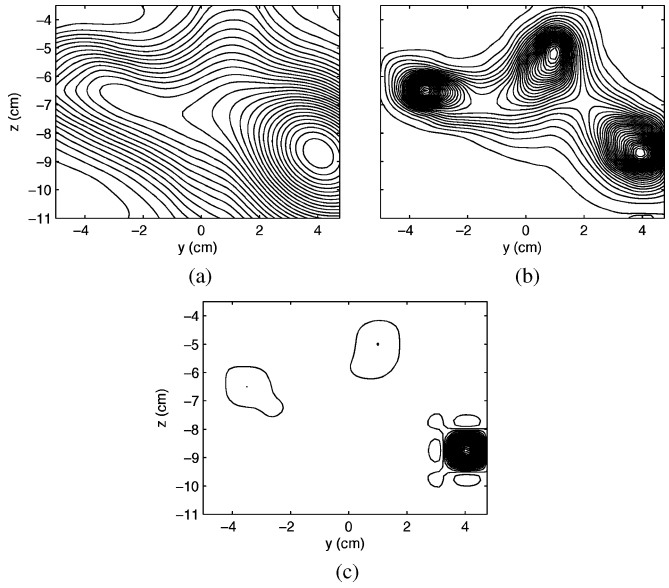

Fig. 6. Results of source reconstruction from the spatiotemporal data in which the first and the second sources are highly correlated. (The correlation coefficient was set to 0.98.) (a) sLORETA spatial filter was used. (b) Proposed AGMN-RUG spatial filter was used. (c) Minimum-variance spatial filter was used. The contours show the relative values of the squared source intensity $\langle|\widehat{\boldsymbol{s}}(\boldsymbol{r},t)|^2\rangle$ on the plane $x = 0$ cm, where $\langle\cdot\rangle$ indicates the average over the 200 time samples.

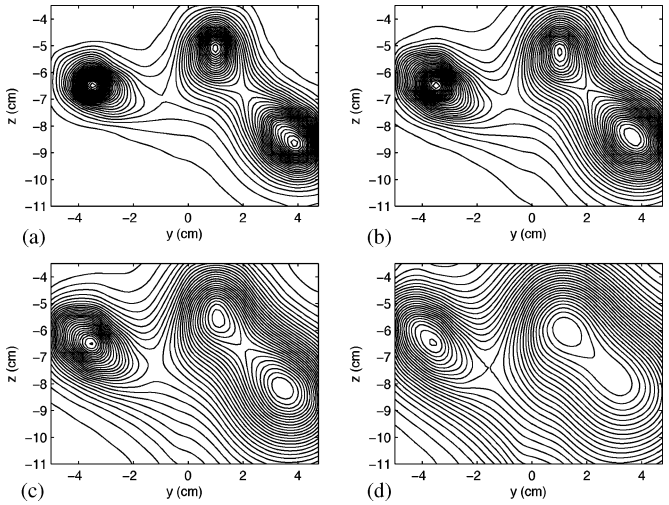

Fig. 7. Results of source reconstruction for four cases of SNR. Other data-generation conditions were the same as those for Fig. 5. (a) Results when SNR was set at eight. (b) Results when SNR set at four. (c) Results when SNR set at two. (d) Results when SNR set at one. The contours show the relative values of the squared source intensity $\langle|\widehat{\boldsymbol{s}}(\boldsymbol{r},t)|^2\rangle$ on the plane $x = 0$ cm, where $\langle\cdot\rangle$ indicates the average over the 200 time samples.

It can be seen that sLORETA again produces rather blurred results and fails to reconstruct the second source. The proposed spatial filter and the minimum-variance spatial filter, however, are successfully able to reconstruct the three sources. The results of the proposed method have a spatial resolution intermediate to those of sLORETA and of the minimum-variance filter. The reconstructed time courses of the three sources appear in Fig. 5(d). These time courses are the reconstructed voxel time courses obtained by the proposed AGMN-RUG spatial filter; the voxels are those that give the three maxima seen in Fig. 5(b). The results demonstrate that the method is capable of providing considerably accurate time-course reconstruction.

We then performed experiments in which sources were highly correlated. Without changing the time courses of the second and the third sources, we assigned the time course $s_1'(t)$ to the first source, obtained using $s_1'(t) = (1-\alpha)s_1(t) + \alpha s_2(t)$, where α controls the degree of correlation between the first and the second sources. This α was set to 0.8, and the correlation coefficient between $s_1'(t)$ and $s_2(t)$ turned out to be 0.98. The results of the source reconstruction, in this case, are shown in Fig. 6. The results of the minimum variance filter show a severe influence from the source correlation known as signal cancellation [4], i.e., the intensities of the first and second sources are significantly diminished. On the other hand, the results of the proposed AGMN-RUG spatial filter show nearly no influence of the source correlation, thereby demonstrating the robustness of the proposed spatial filter to highly correlated sources.

We finally checked the performance of the proposed spatial filter when SNR is considerably low. Here, other conditions for data generation were the same as those for Fig. 5. The reconstruction results from the proposed spatial filter for four cases of SNR are shown in Fig. 7. Results when SNR was set at eight, four, two, and one are, respectively, presented in Fig. 7(a), (b), (c), and (d). These results show that the spatial resolution is affected by the measurement SNR. When SNR is equal to one, the second and the third sources, which are approximately 5-cm apart, are not resolved.

V. Experiments Using Auditory-Evoked MEG Data

The effectiveness of the proposed spatial filter was further tested using auditory-evoked MEG. Measurements were performed using the 160-channel MEG-VISION whole-cortex biomagnetometer (Yokogawa Electric, Inc., Tokyo, Japan). Here, a 1-kHz pure tone of 500 ms duration was delivered to the subject's left ear, and the auditory-evoked field was measured at a sampling rate of 10 kHz. The average interstimulus interval was 2 s. An online low-pass filter with a cutoff frequency of 2 kHz was applied. A total of 400 trials were measured and averaged. The averaged waveforms of the auditory-evoked field are shown in Fig. 8(a).

A single-time-sample data at the latency of 120 ms was used for the reconstruction experiments. This time point, indicated by a vertical broken line in Fig. 8(a), is close to the peak vertex of the M100, and the auditory cortices in the left and right hemispheres are expected to be simultaneously active at this instant. This is confirmed by the contour plots [see Fig. 8(b)] of the sensor data at this time point, because the dipolar patterns are visible above the left and right hemispheres. The results of the reconstruction experiments are shown in Fig. 9. In this figure, the reconstructed source distributions are overlaid onto the sagittal, coronal, and axial slices of the subject MRI.

The results of the minimum-variance filter are shown in Fig. 9(a). To obtain these results, the sample covariance matrix was computed using a time window between 0 and 300 ms, and

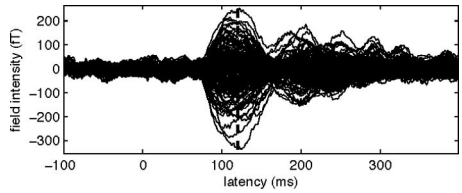

(a)

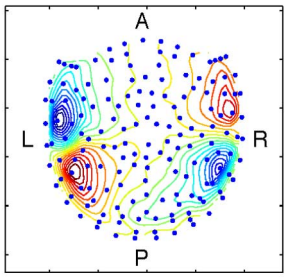

(b)

Fig. 8. (a) Averaged waveforms of the auditory-evoked field used for the reconstruction experiments. The vertical broken line indicates the latency at 120 ms. (b) Sensor-field map at a latency of 120 ms. The contours show the relative intensity of the measured magnetic field. The letters, A, P, L, and R, respectively, show the anterior, posterior, left-hemisphere, and right-hemisphere directions.

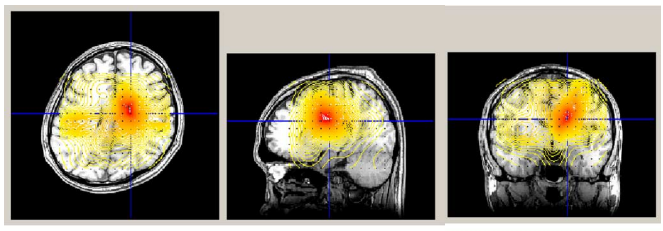

(a)

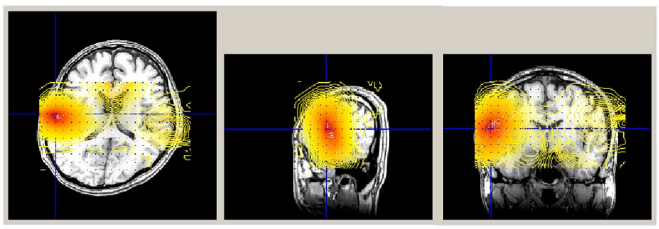

(b)

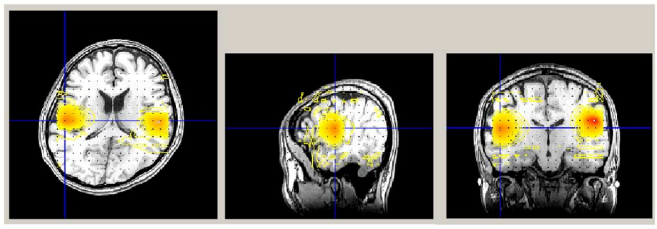

(c)

Fig. 9. Results of the source reconstruction for the auditory-evoked field shown in Fig. 8. The reconstruction results are superimposed onto the subject's MRI, and the axial, sagittal, and coronal slices are shown in the left, middle, and right panels. These slices were chosen as the slices that contained the maximum source intensity. (a) Results obtained from the minimum-variance spatial filter. The source power distribution obtained by averaging the squared source intensity over the time window between 0 and 300 ms is shown. (b) Results obtained from the sLORETA spatial filter. (c) Results obtained from the proposed AGMN-RUG spatial filter. The two sets of results in (b) and (c) were obtained using the single-time-sample data at 120 ms.

the source power distribution (obtained by averaging the squared source intensity over this time window) is shown in Fig. 9(a). In these results, the minimum-variance spatial filter fails to reconstruct the sources of the bilateral activation of auditory cortices, probably because the activities in these cortices are highly correlated. The results from sLORETA are shown in Fig. 9(b) and the results from the proposed spatial filter are shown in Fig. 9(c). Those in Fig. 9(b) and (c) were obtained using the single-time-sample data at 120 ms. The results of sLORETA are significantly blurred and biased. On the contrary, the proposed AGMN-RUG spatial filter can reconstruct the bilateral activities of the auditory cortices with significantly high spatial resolution.

VI. Discussion

We have mentioned that Eq. (26) is used to compute $\bar{\boldsymbol{G}}$ in the update process. However, instead, we can also use

$$\bar{\boldsymbol{G}} = \int_{\Omega} \boldsymbol{L}(\boldsymbol{r}) \,\mathrm{diag}\left[\widehat{\boldsymbol{s}}(\boldsymbol{r},t)\widehat{\boldsymbol{s}}^{T}(\boldsymbol{r},t)\right] \boldsymbol{L}^{T}(\boldsymbol{r})\, d^{3}r \tag{31}$$

where $\mathrm{diag}[\boldsymbol{A}]$ indicates the diagonal matrix whose diagonal elements are equal to those of a matrix $\boldsymbol{A}$. In this case, $\bar{\boldsymbol{G}}$ approaches to the model covariance matrix for a case in which at each source location there are three independent sources whose powers are equal to $\langle s_x(\boldsymbol{r},t)^2\rangle$, $\langle s_y(\boldsymbol{r},t)^2\rangle$, and $\langle s_z(\boldsymbol{r},t)^2\rangle$. We found that (31) gives, in most cases, spatial resolution higher than that from (26), although the difference is generally small. Therefore, we have used (31) in our experiments in Sections IV and V.

To derive the proposed spatial filter, we used the optimization formulation in (22). A slight modification of this formulation is capable of providing another type of recursively implemented spatial filter, which is derived using

$$\begin{aligned}\boldsymbol{W}(\boldsymbol{r}) = \underset{\boldsymbol{W}(\boldsymbol{r})}{\arg\min}\, \mathcal{F}(\boldsymbol{W}), \qquad &\text{subject to} \\ \int_{\Omega} \left[\boldsymbol{W}^{T}(\boldsymbol{r})\boldsymbol{L}(\boldsymbol{r}')\right] \boldsymbol{P}(\boldsymbol{r}') \left[\boldsymbol{W}^{T}(\boldsymbol{r})\boldsymbol{L}(\boldsymbol{r}')\right]^{T} d^{3}r' \\ = \boldsymbol{P}(\boldsymbol{r}) \end{aligned} \tag{32}$$

where the cost function $\mathcal{F}(\boldsymbol{W})$ is defined as

$$\begin{aligned}\mathcal{F}(\boldsymbol{W}) = \int_{\Omega} \mathrm{tr}\{\left[\boldsymbol{W}^{T}(\boldsymbol{r})\boldsymbol{L}(\boldsymbol{r}') - \delta(\boldsymbol{r}-\boldsymbol{r}')\boldsymbol{I}\right] \\ \boldsymbol{P}(\boldsymbol{r}') \left[\boldsymbol{W}^{T}(\boldsymbol{r})\boldsymbol{L}(\boldsymbol{r}') - \delta(\boldsymbol{r}-\boldsymbol{r}')\boldsymbol{I}\right]^{T}\} d^{3}r'. \end{aligned} \tag{33}$$

By setting $\boldsymbol{P}(\boldsymbol{r}) = |\widehat{s}(\boldsymbol{r},t)|^{2}\boldsymbol{I}$, the resultant spatial filter is expressed as

$$\boldsymbol{W}(\boldsymbol{r}) = |\widehat{s}(\boldsymbol{r},t)|\bar{\boldsymbol{G}}^{-1}\boldsymbol{L}(\boldsymbol{r}) \left[\boldsymbol{L}^{T}(\boldsymbol{r})\bar{\boldsymbol{G}}^{-1}\boldsymbol{L}(\boldsymbol{r})\right]^{-1/2}. \tag{34}$$

The spatial filter in Eq. (34) is very similar to the method known as the sLORETA-FOCUSS algorithm [10], [11].[1]

[1]Strictly speaking, the sLORETA-FOCUSS algorithm described in [10] and [11] is different from the recursive spatial filter given in (34), because the algorithm in [10] and [11] uses the sLORETA method only for the initial iteration, and uses the weighted minimum-norm method for other iterations. In contrast, in (34), the sLORETA method is used for all iterations with the weighting of $|\widehat{s}(\boldsymbol{r},t)|$ obtained in the preceding iteration.

The difference between the spatial filter derived above and the proposed AGMN-RUG filter is that the previous spatial filter explicitly contains the estimated source distribution $\widehat{s}(\boldsymbol{r}, t)$ in the weight equation. Therefore, the method generally gives a so-called sparse solution. On the contrary, in the proposed AGMN-RUG spatial filter, the filter weight is updated in an indirect manner, only through the updated gram matrix, and the sparsity is not imposed on the solution. It may probably be true that the proposed spatial filter is superior in the stability, for example, the stability to the number of iterations as was demonstrated in our computer simulation. On the other hand, the method expressed in (34) can attain the spatial resolution higher than that of the proposed method. A performance comparison between these two methods are currently in progress, and results will be presented in a near future occasion.

It should be pointed out that the weights of spatial filters derived with the array-gain constraint are unitless and the reconstructed source vector has the unit of the magnetic field, i.e., the intensity of the reconstructed source is equal to the dipole moment multiplied by the norm of the lead field at the source location. Therefore, the source dipole moment is retrieved by multiplying the reconstructed source intensity with the inverse of the lead-field norm at each source location.

In summary, we have proposed a novel AGMN-RUG spatial filter, which is developed based on a modified version of the minimum-norm method. The proposed spatial filter uses the estimated theoretical covariance matrix, and is designed to have a performance close to that of the adaptive minimum-variance spatial filter. Since the proposed method does not use a sample covariance matrix, a large number of time samples are not needed. The method is also robust to the source correlation. This robustness is demonstrated in our computer simulation and experiments using auditory-evoked MEG data.

The proposed method, however, cannot generally replace the minimum-variance spatial filter because the proposed method attains a spatial resolution only intermediate to those of sLORETA and of the minimum-variance filter, as was shown in our experiments. Therefore, in situations where the minimum-variance spatial filter can attain its full performance, there should be no advantage of using the proposed method. We are now in the process of conducting a series of experiments which will evaluate the method's performance in various conditions. The results of those experiments will be published in a future occasion.

ACKNOWLEDGMENT

The authors would like to thank H. Tanaka for his help in providing auditory-evoked MEG data. They are also grateful to Dr. D. Palomo for his careful proofreading.

REFERENCES

[1] K. Sekihara and S. S. Nagarajan, *Adaptive Spatial Filters for Electromagnetic Brain Imaging*. Berlin, Germany: Springer-Verlag, 2008.

[2] K. Sekihara, M. Sahani, and S. S. Nagarajan, "Location bias and spatial resolution of adaptive and non-adaptive spatial filters for MEG source reconstruction," *NeuroImage*, vol. 25, pp. 1056–1067, 2005.

[3] B. D. van Veen, W. van Drongelen, M. Yuchtman, and A. Suzuki, "Localization of brain electrical activity via linearly constrained minimum variance spatial filtering," *IEEE Trans. Biomed. Eng.*, vol. 44, no. 9, pp. 867–880, Sep. 1997.

[4] K. Sekihara, S. S. Nagarajan, D. Poeppel, and A. Marantz, "Performance of an MEG adaptive-beamformer technique in the presence of correlated neural activities: Effects on signal intensity and time-course estimates," *IEEE Trans. Biomed. Eng.*, vol. 49, no. 12, pp. 1534–1546, Dec. 2002.

[5] S. S. Dalal, K. Sekihara, and S. S. Nagarajan, "Modified beamformers for coherent ref_pubtitle region suppression," *IEEE Trans. Biomed. Eng.*, vol. 53, no. 7, pp. 1357–1363, Jul. 2006.

[6] M. S. Hämäläinen and R. J. Ilmoniemi, "Interpreting measured magnetic fields of the brain: Estimates of current distributions," Helsinki Univ. Technol., Espoo, Finland, Tech. Rep. TKK-F-A559, 1984.

[7] R. E. Greenblatt, A. Ossadtchi, and M. E. Pflieger, "Local linear estimators for the bioelectromagnetic inverse problem," *IEEE Trans. Signal Process.*, vol. 53, no. 9, pp. 3403–3412, Sep. 2005.

[8] R. D. Pascual-Marqui, "Standardized low resolution brain electromagnetic tomography (sLORETA): Technical details," *Methods Findings Exp. Clin. Pharmacol.*, vol. 24, pp. 5–12, 2002.

[9] J. Sarvas, "Basic mathematical and electromagnetic concepts of the biomagnetic inverse problem," *Phys. Med. Biol.*, vol. 32, pp. 11–22, 1987.

[10] R. Khemakhem, B. Hamida, A. Ahmed-Taleb, and P. Derambure, "New hybrid method for the 3d reconstruction of neuronal activity in the brain," in *Proc. 15th Int. Conf. Syst., Signals Image Process.*, 2008, pp. 405–408.

[11] K. Rafik, B. H. Ahmed, F. Imed, and T.-A. Abdelmalik, "Recursive sLORETA-FOCUSS algorithm for EEG dipoles localization," in *Proc. Conf. Image Process. Theory, Tools Appl.*, Nov. 2008, pp. 1–5.

Isamu Kumihashi received the B.E. degree from Tokyo Metropolitan Institute of Technology, Tokyo, Japan, in 2007, and the M.E. degree from Tokyo Metropolitan University, Tokyo, in 2009.

He is currently with the Department of Systems Design and Engineering, Tokyo Metropolitan University. His research interests include the neuromagnetic source imaging and the reconstruction methods, especially their application to imaging of the cardiac electrical activity.

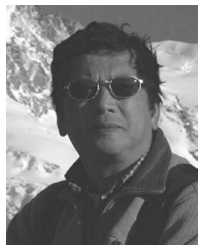

Kensuke Sekihara (M'88–SM'06–F'09) received the M.S. degree in 1976 and the Ph.D. degree in 1987 both from Tokyo Institute of Technology, Tokyo, Japan.

From 1976 to 2000, he was with the Central Research Laboratory, Hitachi Ltd., Tokyo. From 1985 to 1986, he was a Visiting Research Scientist with Stanford University, Stanford, CA. From 1991 to 1992, he was with the Basic Development, Siemens Medical Engineering, Erlangen, Germany. From 1996 to 2000, he was engaged in the "Mind Articulation" research project sponsored by Japan Science and Technology Corporation. He is currently a Professor with the Department of Systems Design and Engineering, Tokyo Metropolitan University, Tokyo. His research interests include the electromagnetic Source imaging, reconstruction and inverse methods, multidimensional signal processing, and statistical signal processing, especially their application to functional Source imaging. He is author of a book *Adaptive Spatial Filters for Electromagnetic Brain Imaging* (Springer-Verlag, 2008).

Dr. Sekihara is a member of the IEEE Medicine and Biology Society and the IEEE Signal Processing Society. He is a Fellow of the International Society of Functional Source Imaging (ISFSI).